

Survival of molecular gas in Virgo's hot intracluster medium: CO near M86

K. M. Dasyra¹, F. Combes¹, P. Salomé¹, and J. Braine^{2,3}

¹ Observatoire de Paris, LERMA, CNRS, 61 Avenue de l'Observatoire, F-75014, Paris, France

² Univ. Bordeaux, Laboratoire d'Astrophysique de Bordeaux, UMR 5804, F-33270, Floirac, France

³ CNRS, LAB, UMR 5804, F-33270, Floirac, France

ABSTRACT

We carried out $^{12}\text{CO}(1-0)$ and $^{12}\text{CO}(2-1)$ observations of 21 different regions in the vicinity of M86, NGC4438, and along the 120 kpc-long, H α -emitting filamentary trail that connects them, aiming to test whether molecular gas can survive to be transferred from a spiral to an elliptical galaxy in Virgo's 10^7K intracluster medium (ICM). We targeted H α -emitting regions that could be associated with the interface between cold molecular clouds and the hot ionized ICM. The data, obtained with the 30m telescope of the Institut de Radioastronomie Millimétrique, led to the detection of molecular gas close to M86. CO gas with a recession velocity that is similar to that of the stars, -265 km s^{-1} , and with a corresponding H_2 mass of $2 \times 10^7 M_\odot$, was detected ~ 10 kpc southeast of the nucleus of M86, near the peak of its HI emission. We argue that it is possible for this molecular gas either to have formed in situ from HI, or to have been stripped from NGC4438 directly in molecular form. In situ formation is nonetheless negligible for the $7 \times 10^6 M_\odot$ of gas detected at 12:26:15.9+12:58:49, at ~ 10 kpc northeast of M86, where no (strong) HI emission is present. This detection provides evidence for the survival of molecular gas in filaments for timescales of ~ 100 Myr. An amount equivalent to $5 \times 10^7 M_\odot$ of H_2 gas that could be lost to the ICM or to neighboring galaxies was also discovered in the tidal tail northwest of NGC4438. A scenario in which gas was alternatively brought to M86 from NGC4388 was also examined but it was considered unlikely because of the non-detection of CO below or at the HI stream velocities, $2000\text{--}2700\text{ km s}^{-1}$.

Key words. (ISM:) evolution — ISM: kinematics and dynamics — ISM: clouds — Galaxies: clusters: individual: Virgo — Galaxies: clusters: intracluster medium — Galaxies: interactions.

1. Introduction

Stripping of gas during galaxy collisions can replenish the gas reservoirs of elliptical galaxies and reinitiate star formation in them, in particular in overdense cluster environments. Cooling flows can further add to the deposition of external gas in cluster ellipticals (see Fabian, 1994, and references therein). The growth of these ellipticals is regulated by the interplay of gas cooling and heating along gas filaments that are associated with either mergers or cooling flows and that have often been discovered in the H α and [N II] images of local clusters (Cowie et al., 1983; Heckman et al., 1989; Conselice et al., 2001; Kenney et al., 2008). This interplay manifests itself and can be examined through the detection of multi-phase gas emission lines in the same clouds. Indeed, warm atomic gas, warm molecular gas, and cold molecular gas clouds have been found to coexist in spatially resolved filaments around NGC1275 (Perseus A), where they were detected through H α , H_2 , and CO emission (Conselice et al., 2001; Salomé et al., 2006, 2011; Johnstone et al., 2007).

Several processes, however, occur in cluster environments that can impede the transfer of gas from one galaxy to another. Ram pressure stripping (Gunn & Gott, 1972), for example, can disperse the diffuse atomic gas into the intracluster medium (ICM). Even though the ram pressure drag is negligible for the motions of the dense molecular gas clouds (Nulsen, 1982; Kenney & Young, 1989), it can even-

tually destroy them by depleting the atomic gas reservoir from which they reform (Crowlet et al., 2005). The molecular clouds are also several orders of magnitude cooler than their environment and can be easily destroyed by X-rays if they are not self-shielded. The ICM X-ray spectrum often peaks in the range 0.7-2.0 keV, indicating temperatures of $\sim 10^7\text{K}$ (e.g., Rangarajan et al., 1995; Machacek et al., 2004; Fabian et al., 2006; Randall et al., 2008; Tamura et al., 2009).

Evidence that molecular clouds do nonetheless survive or reform in $\gtrsim 10^7\text{K}$ intracluster and intragalactic media has been found. Braine et al. (2000) discovered CO in a tidal tail dwarf galaxy of Arp105, in the X-ray emitting medium of Abell 1185 (Mahdavi et al., 1996). Because the CO-emitting regions spatially coincided and had comparable kinematic properties with the HI-emitting regions, Braine et al. (2000) proposed in situ formation of molecules. In addition to the molecular gas detected in the cooling-flow-related filaments around NGC1275 in Perseus (Salomé et al., 2006, 2011; Johnstone et al., 2007), Vollmer et al. (2008) found extraplanar CO near NGC4522 in Virgo, in regions where atomic gas was brought by ram pressure. In ESO137-001, located in Abell 3627, a $\sim 10^7\text{K}$ ram-pressure-driven gas tail has active star formation and H_2 emission (Sun et al., 2010; Sivanandam et al., 2010). In the compact group of Stephan's Quintet, H_2 molecules not only survive in a medium of comparable temperature (Trinchieri et al., 2005;

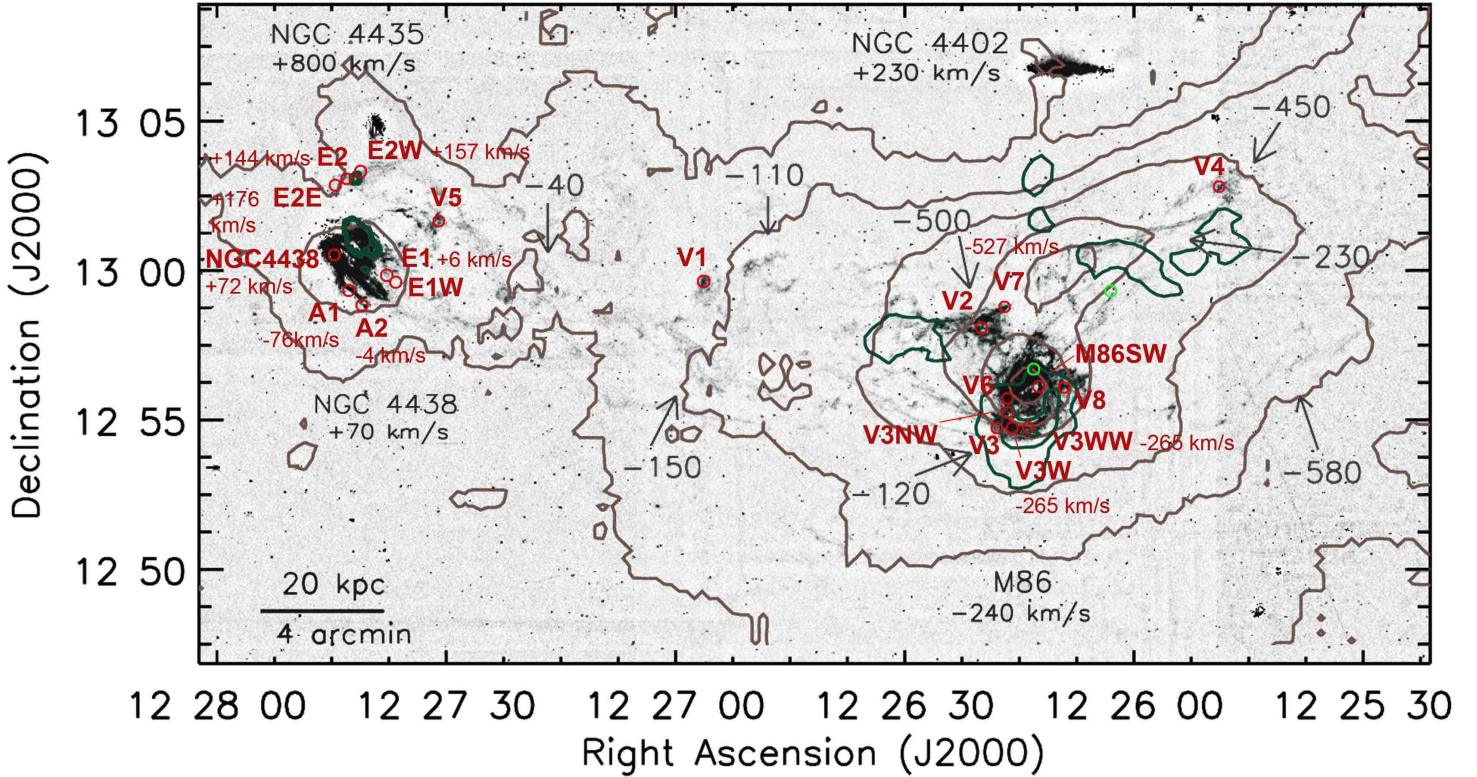


Fig. 1. Finding chart of our observations. The positions of previous CO observations (Wiklind et al. 1995; Braine et al. 1997) are marked with light green circles. HI line contours (dark green) and X-ray contours (brown) are plotted over the narrow band $H\alpha + [N II]$ image of Virgo's core (adapted from Kenney et al. 2008). The velocities appearing in gray correspond to those of the $H\alpha$ gas as measured by the same authors. In red, we mark the $H\alpha$ clouds that we observed searching for associated CO emission. Upon detection, we also indicate the velocity of the molecular gas traced by the $^{12}CO(1-0)$ line. In addition to these 20 regions, we also observed at 12:27:30.0+13:12:12.0, northwest of NGC4435, in the clouds that Cortese et al. (2010a) denote as plume.

O'Sullivan et al., 2009), but they are mainly responsible for the gas cooling instead of the X-rays (Cluver et al., 2010).

An excellent system to test whether molecular gas could be directly brought to an elliptical galaxy, under extreme conditions, from spiral(s) interacting with it is in the Virgo cluster. The dust clumps that are detected in the giant elliptical galaxy M86 (also known as NGC4406) could have originated from its past interaction with its neighboring spiral galaxy NGC4438 (Cortese et al., 2010b; Gomez et al., 2010). Dust and gas could have been captured through ram pressure stripping of the interstellar medium (ISM) of NGC4438 by that of M86 (Kenney et al., 2008), through dynamical instabilities, or through both processes. The HI content deficit of NGC4438 relative to its own CO emission confirms that ram pressure has acted on its ISM (Vollmer et al., 2005, 2009; Hota et al., 2007). Dynamical perturbations continue to distort NGC4438, as indicated by the presence of stars and gas in its northern tidal tail toward NGC4435 (Combes et al., 1988). The interaction between NGC4438 and M86 is confirmed by a spectacular, ~ 120 kpc-long, $H\alpha$ -emitting tidal bridge that connects them (Kenney et al., 2008). The smooth $H\alpha$ velocity gradient along this bridge convincingly places it to the ICM of Virgo, which is rich in X-ray emission (Forman et al., 1979; Rangarajan et al., 1995; Machacek et al., 2004; Liu & Bregman, 2005; Randall et al., 2008). Since the X-ray heating and the ram pressure disperse the ICM atomic gas, a significant fraction of the $H\alpha$ emission could originate from the ionized gas in the

outer layers of molecular clouds (Ferland et al., 2009). This makes the $H\alpha$ clumps in the NGC4438-M86 bridge prime targets for testing whether star formation can be initiated from gas that has either been brought from NGC4438 to M86 in the molecular state, or from molecules that recombined in situ in M86 after being transferred in the atomic state.

We obtained mm data with the 30 m telescope of the Institut de Radioastronomie Millimétrique (IRAM) to test for the presence of molecular gas in some of the $H\alpha$ filaments that are embedded in Virgo's hot ICM. We focused on $H\alpha$ emission peaks, aiming to determine whether the warm atomic gas emission could be associated with cold gas clouds, to compute the amount of molecular gas and potential star formation rate (SFR) in M86, and to test the gas origin by examining whether the molecules could have been transferred there or formed in situ. We assume a distance of 17.5 Mpc to Virgo throughout this work (Mei et al., 2007).

2. Observations and data analysis

The observations were carried out with the 30 m telescope at Pico Veleta, Spain. We observed twenty $H\alpha$ -emitting regions in or near NGC4438 and M86, and along the tidal bridge that connects them (Figure 1), to test whether they contain detectable amounts of CO. In addition to these positions, we also observed clouds in the diffuse, X-ray emit-

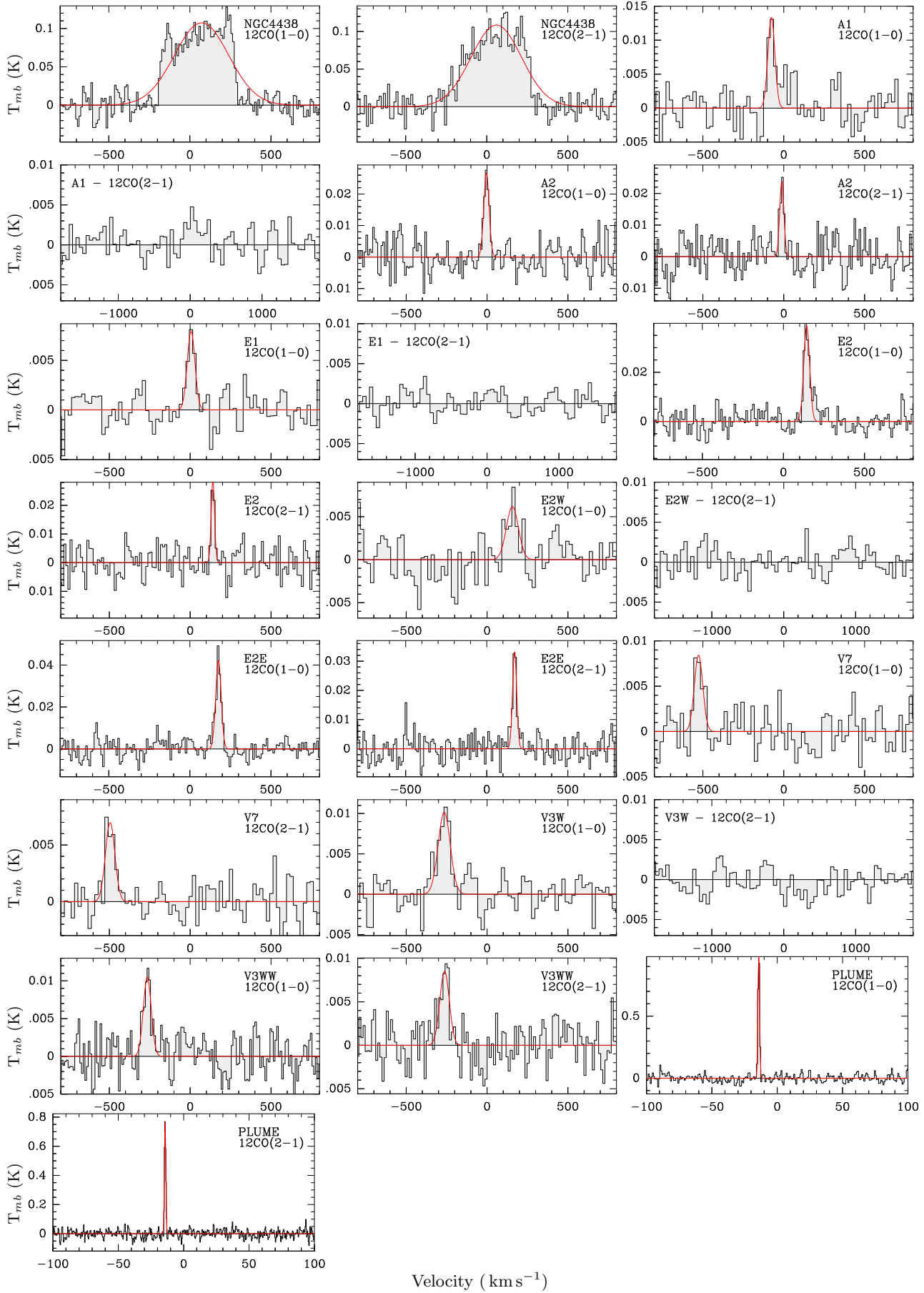


Fig. 2. Spectra of the plume and of the Virgo regions shown in Figure 1 with $^{12}\text{CO}(1-0)$ line detections. Gaussian fits to the CO line profiles (black) are overplotted in red.

Table 1. $^{12}\text{CO}(1-0)$ and $^{12}\text{CO}(2-1)$ line properties and derived gas masses in different Virgo regions.

Position	Coordinates (J2000)	Integration time (min)	Line	$S(\text{CO})^a$ (Jy km s $^{-1}$)	V^b (km s $^{-1}$)	FWHM c (km s $^{-1}$)	T_{mb}^d (mK)	resolution (km s $^{-1}$)	M_{gas}^e (M_{\odot})
NGC4438	12:27:45.60+13:00:32.0	15	$^{12}\text{CO}(1-0)$	226 \pm 6	72 \pm 6	395 \pm 12	108 \pm 14	10	5.7 \times 10 8
NGC4438		15	$^{12}\text{CO}(2-1)$	208 \pm 8	61 \pm 7	362 \pm 14	108 \pm 15	13	...
A1	12:27:43.70+12:59:22.8	110	$^{12}\text{CO}(1-0)$	3.5 \pm 0.6	-76 \pm 5	46 \pm 11	13.4 \pm 3	21	8.8 \times 10 6
A1		109	$^{12}\text{CO}(2-1)$	<5.1	47	...
A2	12:27:42.10+12:58:51.4	25	$^{12}\text{CO}(1-0)$	5.4 \pm 0.6	-4 \pm 2	37 \pm 5	27 \pm 5	10	1.4 \times 10 7
A2		25	$^{12}\text{CO}(2-1)$	3.8 \pm 0.6	-12 \pm 3	29 \pm 6	24 \pm 5	10	...
E1	12:27:38.60+12:59:52.0	90	$^{12}\text{CO}(1-0)$	2.3 \pm 0.4	6 \pm 5	52 \pm 12	7.9 \pm 1.6	21	5.8 \times 10 6
E1		90	$^{12}\text{CO}(2-1)$	<3.8	47	...
E1W	12:27:37.40+12:59:38.3	37	$^{12}\text{CO}(1-0)$	<5.4	47	<3.2 \times 10 6
E1W		37	$^{12}\text{CO}(2-1)$	<3.9	47	...
E2	12:27:44.00+13:03:00.0	50	$^{12}\text{CO}(1-0)$	8.8 \pm 0.7	144 \pm 2	42 \pm 5	39 \pm 3	10	2.2 \times 10 7
E2		50	$^{12}\text{CO}(2-1)$	3.8 \pm 0.7	141 \pm 2	21 \pm 6	29 \pm 5	13	...
E2E	12:27:45.50+13:02:48.0	65	$^{12}\text{CO}(1-0)$	8.7 \pm 0.6	176 \pm 1	38 \pm 3	42 \pm 4	10	2.2 \times 10 7
E2E		65	$^{12}\text{CO}(2-1)$	5.3 \pm 0.6	172 \pm 2	28 \pm 5	33 \pm 4	10	...
E2W	12:27:42.10+13:03:15.0	80	$^{12}\text{CO}(1-0)$	2.6 \pm 0.6	157 \pm 10	84 \pm 22	6.1 \pm 2.1	21	6.5 \times 10 6
E2W		80	$^{12}\text{CO}(2-1)$	<4.8	47	...
V5	12:27:31.60+13:01:38.0	42	$^{12}\text{CO}(1-0)$	<5.4	47	<3.2 \times 10 6
V5		42	$^{12}\text{CO}(2-1)$	<3.8	47	...
V1	12:26:56.20+12:59:40.0	52	$^{12}\text{CO}(1-0)$	<4.7	47	<2.8 \times 10 6
V1		52	$^{12}\text{CO}(2-1)$	<6.4	47	...
V2	12:26:19.00+12:58:10.0	43	$^{12}\text{CO}(1-0)$	<4.7	47	<2.8 \times 10 6
V2		43	$^{12}\text{CO}(2-1)$	<4.1	47	...
V7	12:26:15.90+12:58:49.0	50	$^{12}\text{CO}(1-0)$	2.8 \pm 0.5	-527 \pm 6	59 \pm 12	8.4 \pm 1.9	21	7.1 \times 10 6
V7		45	$^{12}\text{CO}(2-1)$	2.6 \pm 0.4	-495 \pm 6	66 \pm 13	7.0 \pm 1.4	21	...
V4	12:25:47.50+13:02:44.0	23	$^{12}\text{CO}(1-0)$	<6.5	47	<3.9 \times 10 6
V4		23	$^{12}\text{CO}(2-1)$	<4.4	47	...
V3	12:26:17.00+12:54:54.0	37	$^{12}\text{CO}(1-0)$	<5.3	47	<3.1 \times 10 6
V3		37	$^{12}\text{CO}(2-1)$	<5.6	47	...
V3W	12:26:14.90+12:54:54.0	129	$^{12}\text{CO}(1-0)$	4.9 \pm 0.6	-265 \pm 6	89 \pm 15	10 \pm 2	21	1.2 \times 10 7
V3W		129	$^{12}\text{CO}(2-1)$	<4.4	47	...
V3WW	12:26:12.80+12:54:54.0	115	$^{12}\text{CO}(1-0)$	3.2 \pm 0.4	-265 \pm 4	57 \pm 9	11 \pm 2.3	10	8.1 \times 10 6
V3WW		115	$^{12}\text{CO}(2-1)$	3.1 \pm 0.5	-263 \pm 6	68 \pm 16	8.5 \pm 2.2	13	...
V3NW	12:26:15.50+12:55:22.0	40	$^{12}\text{CO}(1-0)$	<8.0	47	<4.7 \times 10 6
V3NW		40	$^{12}\text{CO}(2-1)$	<5.5	47	...
V6	12:26:15.50+12:55:50.0	35	$^{12}\text{CO}(1-0)$	<7.5	47	<4.4 \times 10 6
V6		35	$^{12}\text{CO}(2-1)$	<4.5	47	...
V8	12:26:08.00+12:56:12.0	35	$^{12}\text{CO}(1-0)$	<7.3	47	<4.3 \times 10 6
V8		35	$^{12}\text{CO}(2-1)$	<6.5	47	...
M86SW	12:26:11.40+12:56:15.0	23	$^{12}\text{CO}(1-0)$	<12	47	<7.1 \times 10 6
M86SW		23	$^{12}\text{CO}(2-1)$	<12	47	...
PLUME	12:27:30.00+13:12:12.0	10	$^{12}\text{CO}(1-0)$	8.1 \pm 0.2	-14	1.2	1018 \pm 27	0.8	...
PLUME		10	$^{12}\text{CO}(2-1)$	5.2 \pm 0.1	-14	1.2	782 \pm 27	0.4	...

^(a) Fluxes obtained from the Gaussian fitting to the line profiles, and multiplied by a temperature-to-flux conversion factor of 5.0 Jy/K that is appropriate for the 30m telescope at all observed frequencies. ^(b) All velocities are heliocentric. ^(c) Resolution-corrected line width. ^(d) All limits are computed at 3σ levels. ^(e) A standard CO-to-H $_2$ Galactic value of 4.6 M_{\odot} (K km s $^{-1}$ pc 2) $^{-1}$ was used for the mass computation. The 3σ limits were computed for a width of 47 km s $^{-1}$. This is close to the median $^{12}\text{CO}(1-0)$ width for all regions but the plume and NGC4438.

ting plume northwest of NGC4438 and NGC4435, which is most likely attributed to Galactic cirrus (Cortese et al., 2010a).

We simultaneously observed the ^{12}CO J=1–0 and J=2–1 lines with the EMIR receivers. The receivers were tuned to the frequencies of the two transitions at 115.271 GHz and 230.538 GHz, respectively, shifted to the velocity of the H α gas in each position. All of the 4MHz, WILMA, and VESPA backends, with corresponding resolutions of 4 MHz, 2 MHz, and 0.3 MHz, were simultaneously attached to allow consistency checks, with the WILMA data being primarily used in this work. VESPA data are only shown for the plume. The observations were performed in wobbler-switching mode with a throw of 2'.40. The telescope pointing was monitored by observing a bright radio source every two hours, indicating a pointing accuracy of 2'' to 3''. The

system temperature varied from 270 to 500 K at 3 mm. We typically spent 0.25-2 hours on source, which led to 1σ noise levels of 2 mK to 10 mK at the frequency of the $^{12}\text{CO}(1-0)$ transition (Table 1).

The data were reduced with the CLASS software of IRAM. We averaged the spectra of each region after removing bad channels and subtracting linear baselines, dropping scans with baseline fluctuations. The resulting spectra, binned to 10-21 km s $^{-1}$ channels, are shown in Figure 2. For the plume, the high-resolution VESPA spectra are unbinned. A Gaussian function was fitted to each line for the derivation of its width, peak position, temperature T , and flux S , which are all shown in Table 1. Assuming that the observed clouds are unresolved, T corresponds to the main beam temperature. It was converted to a flux using a

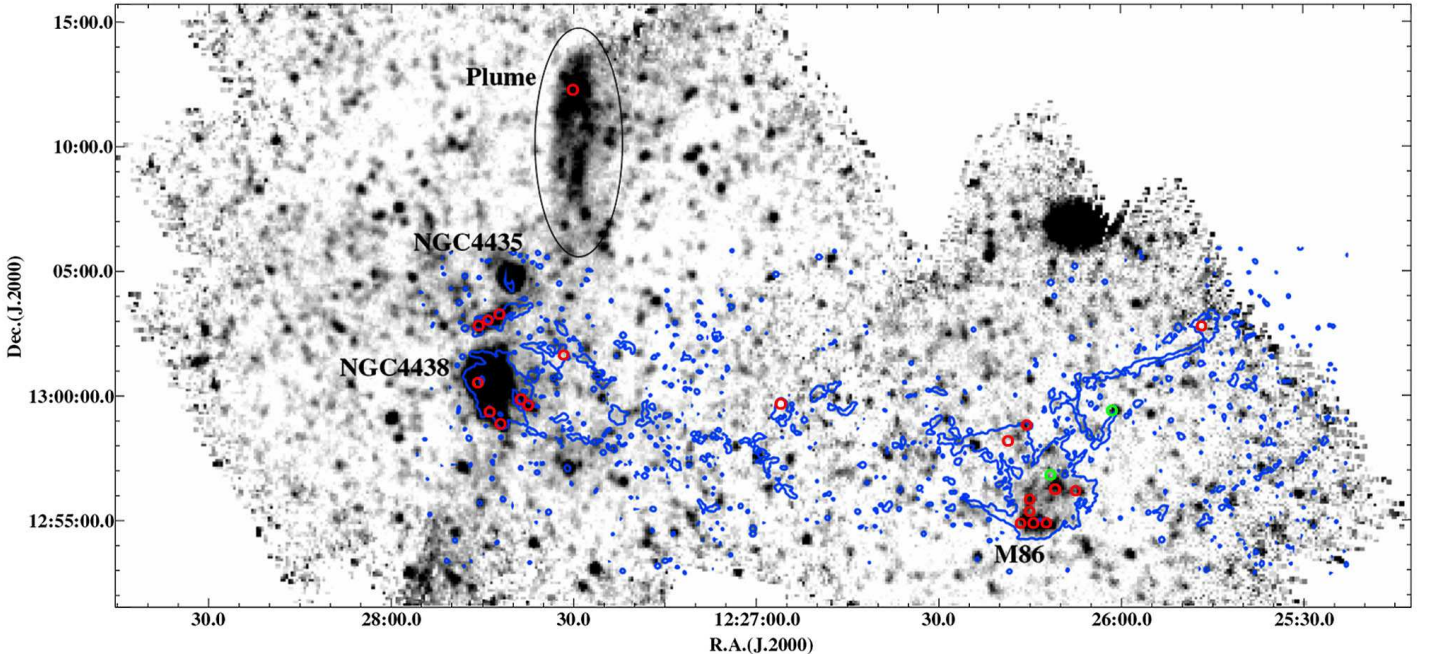


Fig. 3. Our CO observation positions (red circles) and positions of previous CO observations (Wiklind et al. 1995; Braine et al. 1997; green circles), over *Herschel* 250 μm SPIRE imaging data (adapted from Cortese et al. 2010b). The $\text{H}\alpha$ intensity contours are overplotted in blue.

temperature-to-flux conversion factor of 5.0 Jy/K (appropriate for both the 1 and 3 mm observations).

The cold H_2 gas masses, which are also presented in Table 1, were computed as

$$M_{\text{H}_2} = \alpha \frac{23.5 I_{\text{CO}} \Omega_B D_L^2}{(1+z)^3} M_\odot, \quad (1)$$

where I_{CO} is the 115GHz line intensity in K km s^{-1} , Ω_B is the main beam area in arcsec^2 (for unresolved clouds), D_L is the luminosity distance in Mpc, and α is the CO luminosity to H_2 mass conversion factor (Solomon et al., 1997). We used a standard Galactic conversion factor of $4.6 M_\odot (\text{K km s}^{-1} \text{pc}^2)^{-1}$ (Bloemen et al., 1986; Downes et al., 1993), and a telescope beam of $22''$ (i.e., 1.8 kpc) at 3 mm. The 3σ mass limits for non-detections were computed using a resolution (and width) of 47 km s^{-1} , which is characteristic of the clouds under examination (see Table 1).

3. Results: CO-emitting vs non-emitting regions

Narrow $^{12}\text{CO}(1-0)$ and $^{12}\text{CO}(2-1)$ emission is found in the plume clouds northwest of NGC4438 and NGC4435, at $12:27:30+13:12:12$. Both line widths are of only 1.2 km s^{-1} , confirming that the emission originates from Galactic cirrus clouds. This possibility was suggested by Cortese et al. (2010a) based on the $^{12}\text{CO}(1-0)$ line width at a nearby position, $12:27:30+13:12:29$. CO lines were detected in another 10 of the 20 regions shown in Figure 1, but their kinematics were atypical of cirrus clouds, with line width(s) exceeding 30 km s^{-1} in all cases. A cross examination of the high-resolution VESPA data confirms this finding.

Several regions in Virgo, at $\sim 10 \text{ kpc}$ from the B -band center of M86 (at $12:26:12+12:56:49$) had a CO detection.

The region V7, which is located 11 kpc northeast of M86 and in the northwest tip of the local $\text{H}\alpha$ filamentary structure (Fig. 1), contains $7.1 \times 10^6 M_\odot$ of gas that is moving at -527 km s^{-1} . This is very close to the measured $\text{H}\alpha$ recession velocity, -500 km s^{-1} (Kenney et al., 2008). This line-of-sight velocity precludes a clear answer to the question of whether the clouds are bound to M86. The escape velocity at a distance of 10 kpc from the center of M86 is high, 470 km s^{-1} , because its bulge mass equals $2.6 \times 10^{11} M_\odot$. The latter is given in units of $10^{10} M_\odot$ by $c_2 \sigma_{100}^2 R_{\text{eff}}$, where c_2 is a unitless coefficient depending on the matter distribution, σ_{100} is the stellar velocity dispersion in units of 100 km s^{-1} , and R_{eff} is the effective radius in kpc. The value of c_2 for giant ellipticals is 1 (Bender et al., 1992). For M86, σ_{100} is 2.2 (Smith et al., 2000) and R_{eff} is 5.5 kpc (Gavazzi et al., 2005) in the B band.

CO gas was also found in the V3W and V3WW regions, along an $\text{H}\alpha$ stream that results in the center of M86, at 9 to 10 kpc away from it (Figure 1). The CO emission coincides with the HI emission peak of M86 (Li & van Gorkom, 2001; Kenney et al., 2008). The recession velocity of the CO, -265 km s^{-1} , agrees well with that measured from the HI, -240 km s^{-1} (Bregman & Roberts, 1990), and from the Mg stellar absorption features in optical wavelengths, -244 km s^{-1} (Smith et al., 2000). The $^{12}\text{CO}(1-0)$ FWHM in these regions, $50\text{--}90 \text{ km s}^{-1}$, is comparable with the narrow HI component FWHM, 60 km s^{-1} (Bregman & Roberts, 1990). The combined H_2 mass for both V3W and V3WW regions is $2.0 \times 10^7 M_\odot$. If stars are forming out of this gas, and if the galaxy-integrated SFR calibration of Gao & Solomon (2004) is applicable for these clouds, then the SFR will be $0.03 M_\odot \text{ yr}^{-1}$. Likewise, the combination of the modified black body fit to SPIRE data (Cortese et al., 2010b, Figs. 3 and 4) of the same regions that was performed by Gomez et al. (2010) and the Kennicutt (1998)

relation lead to a dust-based SFR estimate that is also on the order of $0.01 M_{\odot} \text{ yr}^{-1}$.

No molecular gas was found at their neighboring V3, V3NW, V6, V8, and M86SW regions. The latter is along the same $\text{H}\alpha$ stream connecting V3W and V3WW to the very center of M86. For $T < 12 \text{ mK}$ and for a line width of 47 km s^{-1} , the gas mass in M86SW is $< 7 \times 10^6 M_{\odot}$. Molecular gas has not been detected at the center of M86 either (Wiklind et al., 1995; Braine et al., 1997); if it exists, its mass must be below $5 \times 10^6 M_{\odot}$ for the assumptions in this work.

No gas was found either at V1, V2, and V5 of the tidal bridge between NGC4438 and M86, or at V4, which is located in the figure-of-eight shaped $\text{H}\alpha$ loop northwest of M86¹. If gas does exist in any of these regions, its mass is below $4 \times 10^6 M_{\odot}$. Previous observations by Wiklind et al. (1995) at another location of this loop, 12:26:02+12:59:21, also led to a non-detection, with an upper limit of $7.9 \times 10^6 M_{\odot}$.

Most of the CO gas is detected in or around NGC4438. At the center of NGC4438, the telescope beam encompasses $6 \times 10^8 M_{\odot}$ of H_2 gas that has a recession velocity identical to that of the $\text{H}\alpha$. The $^{12}\text{CO}(1-0)$ line profile also agrees well with that found from previous observations by Vollmer et al. (2005). Both the $^{12}\text{CO}(1-0)$ and the $^{12}\text{CO}(2-1)$ profiles indicate that the gas is in a disk whose rotational velocity reaches 200 km s^{-1} within the inner 4 kpc of NGC4438². New observations are presented here for the gas clouds at E1, and in the regions E2, E2E, and E2W at ~ 10 kpc north of the nucleus. We specifically observed parts of the $\text{H}\alpha$ filament that is oriented perpendicularly to the tidal tail northeast of NGC4438, which was previously observed by Vollmer et al. (2005). The nearest positions of our observations and those of Vollmer et al. (2005) are one beam ($22''$) away. The clouds in the E2 complexes are moving at $+70$ to $+100 \text{ km s}^{-1}$ from systemic velocity along the line of sight. Their total H_2 mass is $5.1 \times 10^7 M_{\odot}$. Their counterparts in the south of the nucleus are named A1 and A2. They contain $2.3 \times 10^7 M_{\odot}$ of H_2 gas, and they are moving at -80 to -150 km s^{-1} from systemic velocity. For both the northern and southern clouds, the observed velocities are consistent with gas that is either part of a rotating disk, or experiencing tidal and ram pressure stripping (Vollmer et al., 2005). If all of these A and E2 cloud complexes are stripped, a considerable (14%) fraction of the gas in the center of NGC4438 (see Table 1) is potentially lost to the ICM and to neighboring galaxies.

4. Discussion: the origin of the molecular gas near M86

Li & van Gorkom (2001) attributed the origin of the H I emission, which peaks near CO-emitting regions, to gas that cooled down from a compressed, shocked, and heated

¹ This loop belongs to Virgo's ICM and part of it could be bound to M86, because its $\text{H}\alpha$ recession velocity ranges from -230 to -450 km s^{-1} .

² The differences in the observed $^{12}\text{CO}(1-0)$ and $^{12}\text{CO}(2-1)$ line properties of other regions, such as E2W, E2, and E2E, can be accounted for by differences in the gas density and excitation properties, or differences in the sensitivity and the beam size of the observations at the two frequencies, if some filaments are resolved.

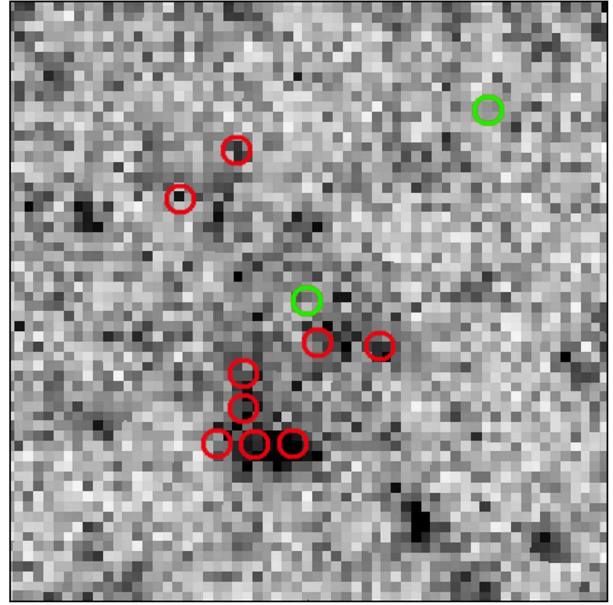


Fig. 4. Our observations plotted over a $4' \times 4'$ zoom around M86 at $350 \mu\text{m}$. The far-infrared image is taken from the first public data release of the *Herschel* Virgo Cluster Survey (HeVICS), which was initially presented in Davies et al. (2010). The CO positions are color-coded as in Figure 3.

medium. In cooling flows, however, the ICM gas is depleted of its dust due to sputtering by X-rays. Dust sputtering leads to gas-to-dust ratios that exceed their typical values for local galaxies (i.e. several hundreds; Young & Scoville, 1991; Wiklind et al., 1995) in timescales of only Myr in 10^6 - 10^7 K environments (Clemens et al., 2010). On the other hand, the presence of dust in all M86 regions where CO was detected (Figs. 3 and 4; Cortese et al., 2010b; Gomez et al., 2010) indicates that the gas and the dust were commonly accumulated. Their relative mass ratio indeed favors the capture from an external galaxy rather than the formation from a cooling ICM. For the inner $2'$ of M86, the total 15 - 20 K dust mass is $(2-5) \times 10^6 M_{\odot}$ (Gomez et al., 2010). If the molecular gas distribution follows the dust distribution, most of the H_2 gas in the inner $2'$ will be accounted for by the observations at V6, V3NW, V3W, V3WW, V8, M86SW, and at the center of M86. The total H_2 mass will then be in the range $(2-5) \times 10^7 M_{\odot}$. Furthermore assuming that the center of M86 comprises $1.1 \times 10^7 M_{\odot}$ of atomic gas based on its $\text{H}\alpha + [\text{N II}]$ luminosity (Kenney et al., 2008), and another $5.6 \times 10^7 M_{\odot}$ based on its H I observations (Bregman & Roberts, 1990), we deduct that its gas-to-dust ratio will be in the range 20 - 60 . The range can be broader when considering the different beam sizes of the observations. For comparison, Cortese et al. (2010b) give a 10 - 20 K dust mass of 2×10^6 - $2 \times 10^7 M_{\odot}$, leading to a gas-to-dust ratio of 30 - 300 (including helium) for a dust knot 5 kpc northwest of NGC4438.

With its $\text{H}\alpha$ -emitting trail, NGC4438 is the best candidate for the external capture of the gas and the dust in M86. While the trail started elongating as the two galaxies were receding from each other, most of the gas and the dust was likely captured when the galaxies were near the pericenter of their encounter. If gas was transferred from NGC4438 to M86 in ionized or neutral state through dy-

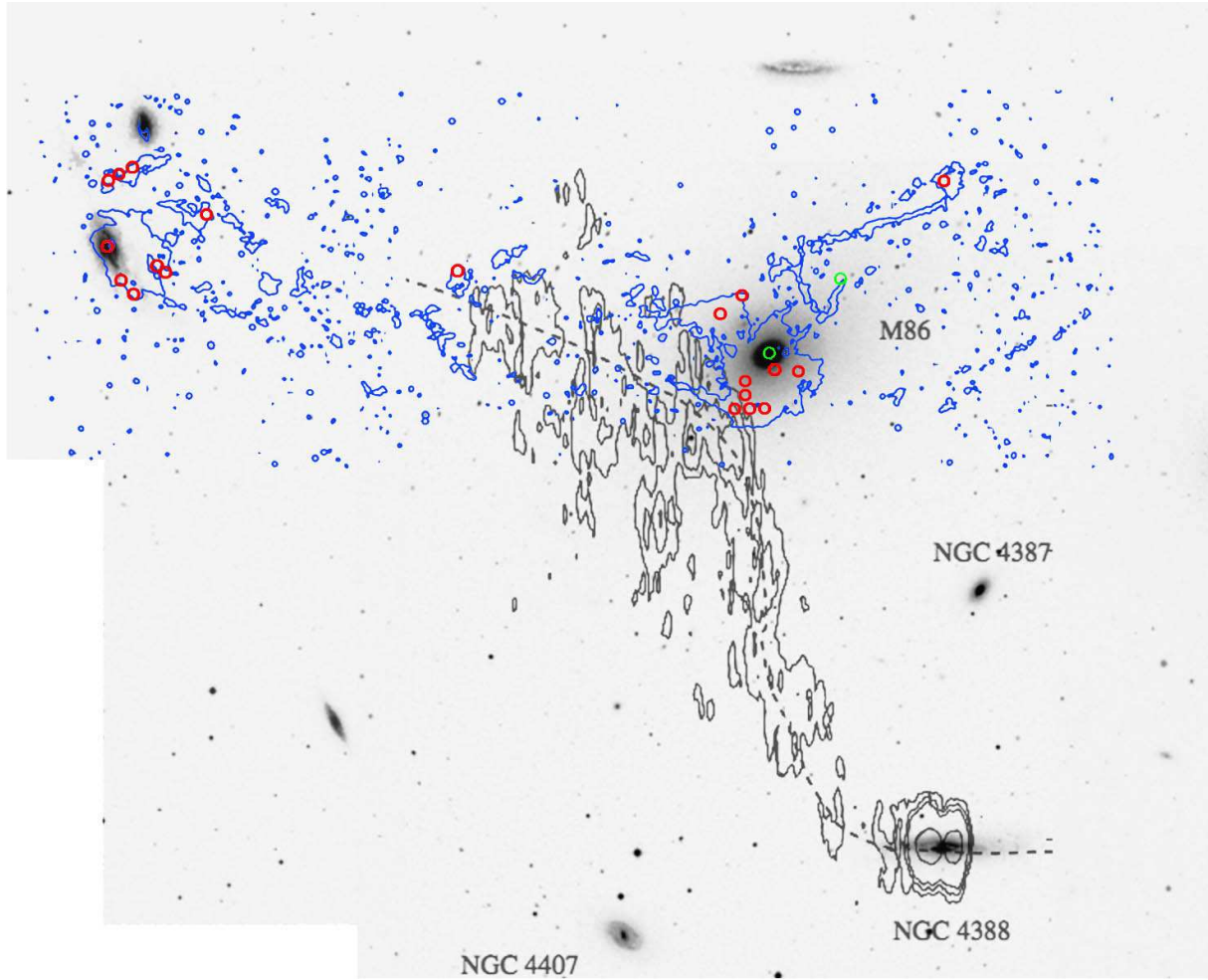


Fig. 5. CO observation positions and H α intensity contours (as in Figure 3) and HI intensity contours (black; Oosterloo & van Gorkom 2005) plotted over a DSS B-band image.

namical instabilities or ISM-ISM stripping, CO could be detected in M86 if it reformed in situ. Molecular formation is possible to occur in situ in the V3W and V3WW complexes. The column density threshold for the efficient conversion of HI to H₂ is in the range $3 \times 10^{20} - 10^{21} \text{ cm}^{-2}$ (Schaye, 2004). The HI-deduced column density in these regions is close to the $1.6 \times 10^{20} \text{ cm}^{-2}$ contour of Kenney et al. (2008). Likewise, the CO-based H₂ column density is 2.9×10^{20} and $1.9 \times 10^{20} \text{ cm}^{-2}$ for V3W and V3WW, respectively, for the adopted CO-to-H₂ Galactic conversion factor. The HI column density requirement would be satisfied if the HI-to-H₂ mass ratio was $\gtrsim 3$, which is comparable to that of both moderately stripped spirals and ellipticals (Kenney & Young, 1989; Wiklind et al., 1995). The present computations assume that the gas emission is smeared out across each telescope's beam. When taking into account the clumpy distribution of the clouds, the column density requirement can be easily met. For this scenario to hold, the CO needs to be detected in regions where dust is also present, because the dust particles act like catalysts for the HI atoms to recombine upon. This condition is also satisfied.

Contrarily to the V3W(W) complexes, the bulk of the molecules could not have formed in situ in V7, where the HI-deduced column density is outside the last contour of

Kenney et al. (2008), i.e., below 10^{19} cm^{-2} . The detection of CO there provides evidence for the survival and transport of self-shielded molecular clouds in the hot ICM of Virgo. The molecules could have started forming, e.g., near the HI peak south of M86 and then rotated around it in a half-circular orbit of $\sim 30 \text{ kpc}$. If the clouds were moving at 300 km s^{-1} (i.e. close to the V3W and V7 difference in recession velocity), their travel time would be 100 Myr. Because the formation of new stars from H₂ in isolated clouds takes place in timescales of $10^5 - 10^7 \text{ yr}$ (e.g., Krumholz et al., 2011), this result implies that the collapse, the fragmentation, and the reformation of the molecular clouds from gas in their vicinity is a continuous process inside filaments.

Alternatively, gas clumps could have been transferred from NGC4438 to M86 directly in a dense, molecular state. The molecular gas has then survived near M86 for a time comparable to the travel time of NGC4438 from the pericenter to its present location. The orbital simulations of Vollmer et al. (2009) also suggest that NGC4438 has been moving through the hot X-ray gas for over only 100 Myr after its encounter with M86. This timescale is insufficient for the various energy/momentum transport processes that act on the molecular clouds to fully destroy them. These processes include the heat conduction from the surrounding medium, the viscous flow stripping, and the Kelvin-

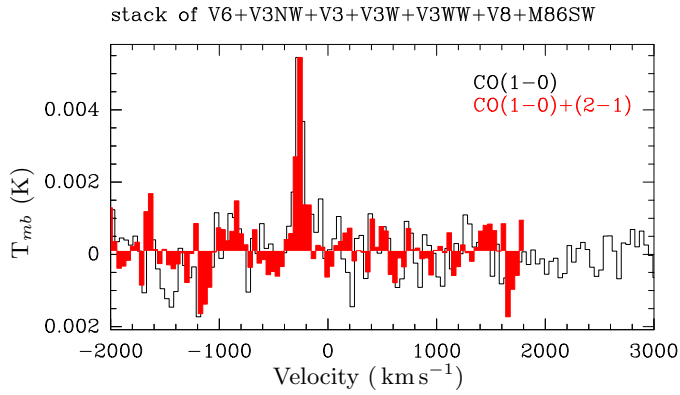


Fig. 6. Stacked spectra of all positions south of M86. No gas is detected at any velocity other than the galaxy's recession velocity.

Helmholtz instabilities, with the heat conduction leading to the highest mass loss rates in this environment (Nulsen, 1982). In the ICM, the mean free path of the electrons is large compared to the radii of the molecular clouds, leading to saturated heat conduction and long evaporation timescales (Cowie & McKee, 1977). For a cloud with radius of 10 pc and density n of 10^3 cm^{-3} that is embedded in a 10^7 K medium with density of 10^{-4} cm^{-3} , the evaporation time is 3 Gyr. This time can increase when magnetic fields and radiative cooling are taken into account (Cowie & McKee, 1977; McKee & Cowie, 1977), because cooling is very efficient above 10^4 K (Dalgarno & McCray, 1972). It effectively dominates over heating for clouds that are stripped outside of galaxies and that are not sufficiently heated by stellar ultraviolet radiation (Vollmer et al., 2001). The atomic gas will then cool down, condense, and reform H_2 within $\sim 10^9/n \text{ yr cm}^{-3}$ (Hollenbach & Tielens, 1997). It is therefore plausible that the molecular gas observed in M86 was directly stripped from NGC4438, even though it was not detected in our observations of, e.g., the V1 region. This might occur if there is no strong source of gas excitation, such as star formation, shocks, cosmic rays (Ferland et al., 2008), or diffuse intracluster light (Mihos et al., 2005).

An entirely different scenario that remains to be tested is whether the gas in M86 could originate from NGC4388, a spiral galaxy at $\sim 100 \text{ kpc}$ in projection on its south, with an estimated H_2 reservoir of 10^8 – $10^9 M_\odot$ (Kenney & Young, 1989; Papadopoulos & Seaquist, 1998). NGC4388 could be interacting with the M86-NGC4438 complex, if all galaxies were at a sufficiently close distance (e.g., Willick et al., 1997). The interaction scenario was considered after the detection of a long ($> 120 \text{ kpc}$) trail of neutral gas starting from NGC4388 and heading in the direction of M86 and NGC4438 (Oosterloo & van Gorkom, 2005, Fig. 5), and by the strong gas stripping in this system (e.g., Kenney & Young, 1989; Vollmer et al., 2009). Very Large Array data indicated that NGC4388 has a radio jet that is driven by an active nucleus (Colbert et al., 1996; Irwin et al., 2000) and that could be adding to the gas expulsion mechanisms. A massive outflow has been observed in its $\text{H}\alpha$ and $[\text{N II}]$ images (Veilleux et al., 1999; Kenney et al., 2008), with an $\text{H}\alpha$ velocity ranging between 2000 km s^{-1} and 2400 km s^{-1} (Yoshida et al., 2004). The velocity of the neutral, H I -emitting gas along the trail is likewise between

2000 – 2700 km s^{-1} (Cayatte et al., 1990; Oosterloo & van Gorkom, 2005; Chung et al., 2009). The projected H I detection limits are close to the $\text{H}\alpha$ detection limits in the vicinity of M86 (Fig. 5). However, the non-detection of CO moving at any velocity between -250 km s^{-1} and 2700 km s^{-1} in the south of M86 (either in individual or stacked spectra; Fig. 6) renders this scenario improbable. A similar conclusion was drawn by Oosterloo & van Gorkom (2005) based on the H I gas kinematics. Additional (and deeper) observations would be needed to test the viability of this scenario.

5. Summary

Using IRAM's 30m telescope, we investigated the presence of molecular gas in Virgo's hot ICM, and specifically in the vicinity of M86, NGC4438, and in the 120 kpc-long tidal trail that connects them. We focused on $\text{H}\alpha$ emission peaks, which could originate from the interface of dense clouds with self-shielded CO molecules and the X-ray emitting ICM, because ram pressure stripping has dispersed most of the diffuse ionized gas. We observed 21 regions in the $^{12}\text{CO}(1-0)$ and $^{12}\text{CO}(2-1)$ transitions and we draw the following main conclusions.

- Narrow CO emission, with line widths of only 1.2 km s^{-1} , was detected at 12:27:30+13:12:12, northwest of NGC4438 and NGC4435. It is tracing Galactic cirrus clouds. In no other position were the CO line widths characteristic of those in the cirrus.
- CO was detected at more than 10 kpc away from the centers of NGC4438 and M86. For example, strong CO emission was found in the tidal structure north of NGC4438, in the regions E2E, E2, and E2W. Through these cloud complexes, $5 \times 10^7 M_\odot$ or 9% of the gas in the center of NGC4438 could be lost to the ICM and potentially to neighboring galaxies.
- CO was discovered in an $\text{H}\alpha$ stream that ends in the center of M86, at $\sim 10 \text{ kpc}$ southeast from the center, and near the peak of the H I emission. The CO recession velocity agrees well with that of the H I and the stars. The $^{12}\text{CO}(1-0)$ line properties indicate the presence of $2 \times 10^7 M_\odot$ of H_2 in the combined regions V3W and V3WW. Some of this gas could have formed in situ given that the local H I surface brightness exceeds 10^{20} cm^{-2} .
- The filamentary structure 11 kpc northeast from the center of M86, in the region that is denoted V7, contains CO moving at -530 km s^{-1} . Its corresponding H_2 mass is $7 \times 10^6 M_\odot$. Because there is no associated H I emission in this region or in its vicinity, we attribute this CO detection to gas that was primarily transferred to V7 in molecular form. We interpret it as survival of self-shielded, re-forming molecular clouds in filaments for $\sim 100 \text{ Myr}$. This is longer than the fragmentation timescale of individual isolated clouds, and shorter than the evaporation timescale due to heat conduction from the ICM.
- The integrated gas-to-dust ratio in the inner $2'$ of M86, 20–60, is too low to be consistent with gas cooling from the ICM. The molecular gas detected in and near M86 is therefore likely to have originated from an external galaxy.
- The most probable scenario for the molecular gas origin of M86 is that it comes from NGC4438. The best evidence for this remains the smooth $\text{H}\alpha$ velocity gradient

in the bridge between them, combined with the similar H α and CO velocities, where detected.

- The scenario of gas being transferred to M86 from NGC4388 on its south was also examined, given the H I stream that is seen in projection between these galaxies. However, the non-detection of CO below or in the observed range of H I recession velocities, i.e., between 2000–2700 km s⁻¹, does not favor this scenario.

Acknowledgements. K. D. acknowledges support by the Centre National d'Etudes Spatiales (CNES). We are thankful to G. Novak for constructive discussions, to the HeVICS team for making their data publicly available, and to the anonymous referee who helped us to improve this document. Based on observations carried out with the IRAM 30 m telescope. IRAM is supported by INSU/CNRS (France), MPG (Germany) and IGN (Spain).

References

- Bender, R., Burstein, D., & Faber, S. M. 1992, ApJ, 399, 462
- Bloemen, J. B. G. M., Strong, A. W., Mayer-Hasselwander, H. A., et al. 1986, A&A, 154, 25
- Braine, J., Henkel, C., & Wiklind, T. 1997, A&A, 321, 765
- Braine, J., Lisenfeld, U., Duc, P.-A., Leon, S. 2000, Nature, 403, 867
- Bregman, J. N., & Roberts, M. S. 1990, ApJ 362, 468
- Cayatte, V., van Gorkom, J. H., Balkowski, C., & Kotanyi, C., 1990 AJ, 100, 604
- Chung, A., van Gorkom, J. H., Kenney, J. D. P., Crowl, H., & Vollmer, B. 2009, AJ, 138, 1741
- Clemens, M. S., Jones, A. P., Bressan, A., et al. 2010, A&A, 518, L50
- Cluver, M. E., Appleton, P., Boulanger, F., et al. 2010, ApJ, 710, 248
- Colbert, E. J. M., Baum, S. A., Gallimore, J. F., O'Dea, C. P., & Christensen, J. A. 1996, ApJ, 467, 551
- Combes, F., Dupraz, C., Casoli, F., & Pagani, L. 1988, A&A, 203, L9
- Conselice, C. J., Gallagher, J. S., III, & Wyse, R. F. G. 2001, AJ, 122, 2281
- Cortese, L., Bendo, G. J., Isaak, K. G., et al. 2010a, MNRAS, 403, L26
- Cortese, L., Bendo, G. J., Boselli, A., et al. 2010b, A&A, 518, L63
- Cowie, L. L. & McKee, C. F., 1977, ApJ, 211, 135
- Cowie, L. L., Hu, E. M., Jenkins, E. B., & York, D. G. 1983, ApJ, 272, 29
- Crowl, H. H., Kenney, J. D. P., van Gorkom, J. H., & Vollmer, B., 2005, AJ, 130, 65
- Dalgarno, A. & McCray, R. A. 1972, ARA&A, 10, 375
- Davies, J. I., Baes M., Bendo G.J., 2010, et al. A&A 518, L48
- Downes, D., Solomon, P. M., & Radford, S. J. E. 1993, ApJ, 414, L13
- Fabian, A. C. 1994, ARA&A, 32, 277
- Fabian, A. C., Sanders, J. S., Taylor, G. B., et al. 2006, MNRAS, 366, 417
- Ferland, G. J., Fabian, A. C., Hatch, N. A., et al. 2008, 386, L72
- Ferland, G. J., Fabian, A. C., Hatch, N. A., et al. 2009, MNRAS, 392, 1475
- Forman, W., Schwarz, J., Jones, C., Liller, W., & Fabian, A. C. 1979, ApJ, 234, L27
- Gao, Y., & Solomon, P. M. 2004, ApJ, 606, 271
- Gavazzi, G., Donati, A., Cucciati, O., et al. 2005, A&A, 430, 411
- Gomez, H. L., Baes, M., Cortese, L., et al. 2010, A&A, 518, L45
- Gunn, J. E., & Gott, J. R. III 1972, ApJ, 176, 1
- Heckman, T. M., Baum, S. A., van Breugel, W. J. M., & McCarthy, P. 1989, ApJ, 338, 48
- Hollenbach, D. J., & Tielens, A. G. G. M. 1997, ARA&A, 35, 179
- Hota, A., Saikia, D. J., & Irwin, J. A. 2007, MNRAS, 380, 1009
- Irwin, J. A., Saikia, D. J., & English, J. 2000, AJ, 119, 1592
- Johnstone, R. M., Hatch, N. A., Ferland, G. J., et al. 2007, MNRAS, 382, 1246
- Kenney, J. D. P., & Young, J. S. 1989, ApJ, 344, 171
- Kenney, J. D. P., Tal T., Crowl H. H., et al. 2008, ApJ, 687, L69
- Kennicutt, R., C., Jr. 1998, ARA&A, 36, 189
- Krumholz, M. R., Dekel, A., & McKee, C. F., 2011, ApJ, in press, arXiv:1109.4150
- Li, Y., & van Gorkom, J. 2001, ASP Conf 240, 637
- Liu, J.-F., & Bregman, J. N., 2005, ApJS, 157, 59
- O'Sullivan, E. O., Giacintucci, S., Vrtilik, J. M., Raychaudhury, S., & David, L. P. 2009, ApJ, 701, 1560
- Oosterloo, T., & van Gorkom, J. 2005, A&A, 437, L19
- Machacek, M. E., Jones, C., & Forman, W. R. 2004, ApJ, 610, 183
- Mahdavi, A., Margaret J., Fabricant, D. G., et al. 1996, AJ, 111, 1
- McKee, C. F., & Cowie, L. L. 1977, ApJ, 215, 213
- Mei, S., Blakeslee, J. P., Côté, P., et al. 2007, ApJ, 655, 144
- Mihos, J. C., Harding, P., Feldmeier, J., & Morrison, H. 2005, ApJ, 631, L41
- Nulsen, P. E. J. 1982, MNRAS, 198, 1007
- Papadopoulos, P. P., & Seaquist, E. R. 1998, ApJ, 492, 521
- Randall, S., Nulsen, P., Forman, W. R., et al. 2008, ApJ, 688, 208
- Rangarajan, F. V. N., White, D. A., Ebeling, H., & Fabian, A. C. 1995, MNRAS, 277, 1047
- Salomé, P., Combes, F., Edge, A. C., et al. 2006, A&A, 454, 437
- Salomé, P., Combes, F., Revaz, Y. et al. 2011, A&A, 531, 85
- Schaye, J. 2004, ApJ, 609, 667
- Solomon, P. M., Downes, D., Radford, S. J. E., & Barrett, J. W. 1997, ApJ, 478, 144
- Sivanandam, S., Rieke, M. J., & Rieke, G. H. 2010, ApJ, 717, 147
- Smith, R. J., Lucey, J. R., Hudson, M. J., Schlegel, D. J., & Davies, R. L., 2000, MNRAS, 313, 469
- Sun, M., Donahue, M., Roediger, E., et al. 2010, ApJ, 708, 946
- Tamura, T.; Maeda, Y.; Mitsuda, K., et al. 2009, ApJ, 705, L62
- Trinchieri, G., Sulentic, J., Pietsch, W., & Breitschwerdt, D. 2005, A&A, 444, 697
- Veilleux, S., Bland-Hawthorn, J., Cecil, G., Tully, R. B., & Miller, S. T. 1999, ApJ, 520, 11
- Vollmer, B., Cayatte, V., Balkowski, C., & Duschl, W. J. 2001, ApJ, 561, 708
- Vollmer, B., Braine, J., Combes, F., & Sofue, Y. 2005, A&A, 441, 473
- Vollmer, B., Braine, J., Pappalardo C., & Hily-Blan, P. 2008, A&A 491, 455
- Vollmer, B., Soida, M., Chung, A., et al. 2009 A&A, 496, 669
- Willick, J. A., Courteau, S., Faber, S. M., et al. 1997, ApJS, 109, 333
- Wiklind, T., Combes, F., & Henkel, C. 1995, A&A, 297, 643
- Yoshida, M., Ohyama, Y., Iye, M., et al. 2004, AJ, 127, 90
- Young, J. S., & Scoville, N. Z. 1991, ARA&A, 29, 581